APPENDIX A

A NOVEL NON-LINEAR SPRING TO MODEL THE GENDER-SPECIFIC QUADRICEPS RESPONSE TO RAPID STRETCH DURING A JUMP LANDING

A.1 Abstract

Active whole muscle exhibits a non-linear force-displacement response to rapid stretch. Since the quadriceps is rapidly lengthened during the initial 100 ms of a jump landing, there is a need to physically simulate its non-linear response when considering muscle loads acting across the knee during simulated jump landings *in vitro*. We designed a custom titanium spring with a prescribed bi-linear load-displacement behavior to model the active female quadriceps muscle-tendon unit tensile stiffness; a supplementary spring was added in parallel to model the 20% greater stiffness of the male quadriceps. The quadriceps spring's performance was first validated quasistatically. Then, eight female knees were mounted in a Withrow-Oh knee testing apparatus and the male and female quadriceps spring forces were measured dynamically using a uniaxial load cell during two-times body weight simulated non-pivot and pivot landings. A 2 x 2 ANOVA was used to analyze the effect of landing type and quadriceps stiffness on peak quadriceps force within our testing apparatus. The female and male quadriceps springs had initial stiffnesses of 155 N/mm and 193 N/mm, respectively, and final stiffnesses of 27 N/mm and 46 N/mm, respectively. Pivot landings resulted in a significantly greater peak quadriceps force than non-pivot landings ($p = 0.013$), and the male quadriceps

spring tended to exhibit a greater peak quadriceps force than the female spring ($p = 0.104$). We conclude that it is possible to physically simulate the rapid non-linear stretch responses of the female and male quadriceps during simulated jump landings in cadaver knee preparations.

A.2 Introduction

During a jump landing, the quadriceps muscle undergoes rapid stretch during the initial 100 ms of the knee flexion phase of the landing, as the knee flexes from 20^{o} knee flexion at initial ground contact to 60^{o} knee flexion at peak ground reaction force[17]. The previous *in vitro* Withrow-Oh knee apparatus modeled the stretch behavior of the quadriceps muscle with a linear stiffness using aircraft cable[20] or with braided nylon string[14]. However, a linear force-deformation curve fails to represent the characteristic non-linear change in force as striated muscle is suddenly lengthened. For example, active single striated muscle fibers with an initial length on the plateau region or descending limb of the sarcomere length-tension curve are known to exhibit a non-linear force–length behavior under rapid stretch with a steep initial positive slope, followed by no force enhancement or residual force enhancement as the muscle fiber continues to stretch[1, 2, 8]. A corresponding bi-linear response has been shown in whole muscle[6]. We therefore surmise that quadriceps will demonstrate a non-linear force-displacement response during the first 100 ms of the knee flexion phase during a single limb landing.

We developed a non-linear quadriceps spring unit for the Withrow-Oh *in vitro* knee apparatus. This spring unit exhibits the calculated *in vivo* behavior of the quadriceps muscle-tendon unit (henceforth 'quadriceps') during the initial 100 ms of rapid lengthening during a jump landing. The spring unit has interchangeable springs to model

both male and female *in vivo* quadriceps tensile stiffness values because of their 20% different stiffnesses[5]. The non-linear springs were validated quasistatically via the measured force-length relationship of the springs, and then dynamically tested on the Withrow-Oh apparatus during simulated two-times body weight (2*BW) pivot and non-pivot landings.

A.3 Materials and Methods

Non-linear springs with a prescribed load-displacement function have been previously described[9, 10]. Briefly, the in-plane (2-mm) and out-of-plane spring thicknesses (19.1 mm and 27.0 mm for female and male quadriceps spring, respectively) were defined. The theoretical bi-linear load-displacement relationship for the spring was designed with ANSYS (v11, ANSYS Inc., Canonsburg, PA) to exhibit a high initial stiffness and lower final stiffness, similar to the known whole muscle's *in vivo* response to rapid stretch. Deforming the spring with a one degree-of-freedom movement produced the desired bi-linear characteristic of the intact *in vivo* muscle. Several springs were mounted in parallel to represent the female quadriceps, with supplementary springs being added in parallel to develop the 20% larger initial stiffness of the male quadriceps stiffness[5] and strength[16].

The "J-shaped" springs were fabricated with a water jet cutter from high-strength titanium alloy (Ti-6Al-4V). To reduce fabrication costs, we cut separate springs from thin sheets of titanium (6.35 mm, 3.18 mm, and 1.59 mm thick). The requisite number of springs was then mounted in parallel to obtain the desired performance. A custom aluminum housing constrained the ends of the spring to deform collinearly (Figure A.1). The "base" female quadriceps spring consisted of three parallel 6.35 mm-thick titanium

springs. Two 9-mm diameter steel pins prevented translation and rotation of the spring's proximal end, while a third pin connected the spring's distal end to a lubricated slider that constrained translation distally. To represent the male quadriceps spring, an additional aluminum plate with one 3.18 mm and one 1.59 mm-thick titanium spring was added in parallel to the base housing (Figure A.1).

The static load-displacement spring function was measured using a custom-testing uniaxial rig that slowly stretched the springs within the housing while recording the spring's displacement and output force at 100 Hz using two optoelectronic markers (Optotrak Certus, Northern Digital Inc., Waterloo, ON, Canada) and an in-series uniaxial load cell (TLL-1K, Transducer Techniques, Inc, Temecula, California). The dynamic force-time responses of the male and female non-linear quadriceps springs were compared in eight female knees (age: 67 (20) yrs; height: 172 (3) cm; body mass: 68 (5) kg) using the Withrow-Oh dynamic *in vitro* lower extremity testing apparatus with realistic muscle loads[11]. Five non-pivot (compression + flexion moment) and five pivot (same loading + internal tibial torque) 2*BW simulated landings were performed on each knee. The rectus femoris tendon was attached to the spring housing with a cryo-clamp and pre-tensioned to 200 N prior to each trial to maintain an initial 15^{o} knee flexion angle. Quadriceps spring tension during the landing was monitored at 2 kHz using an in-series uniaxial load cell. Assuming normality, 2 x 2 ANOVA was performed in SPSS 19 (IBM Corp., Armonk, NY) compared the effects of quadriceps spring stiffness and landing type on peak quadriceps force. $P<0.05$ was considered significant.

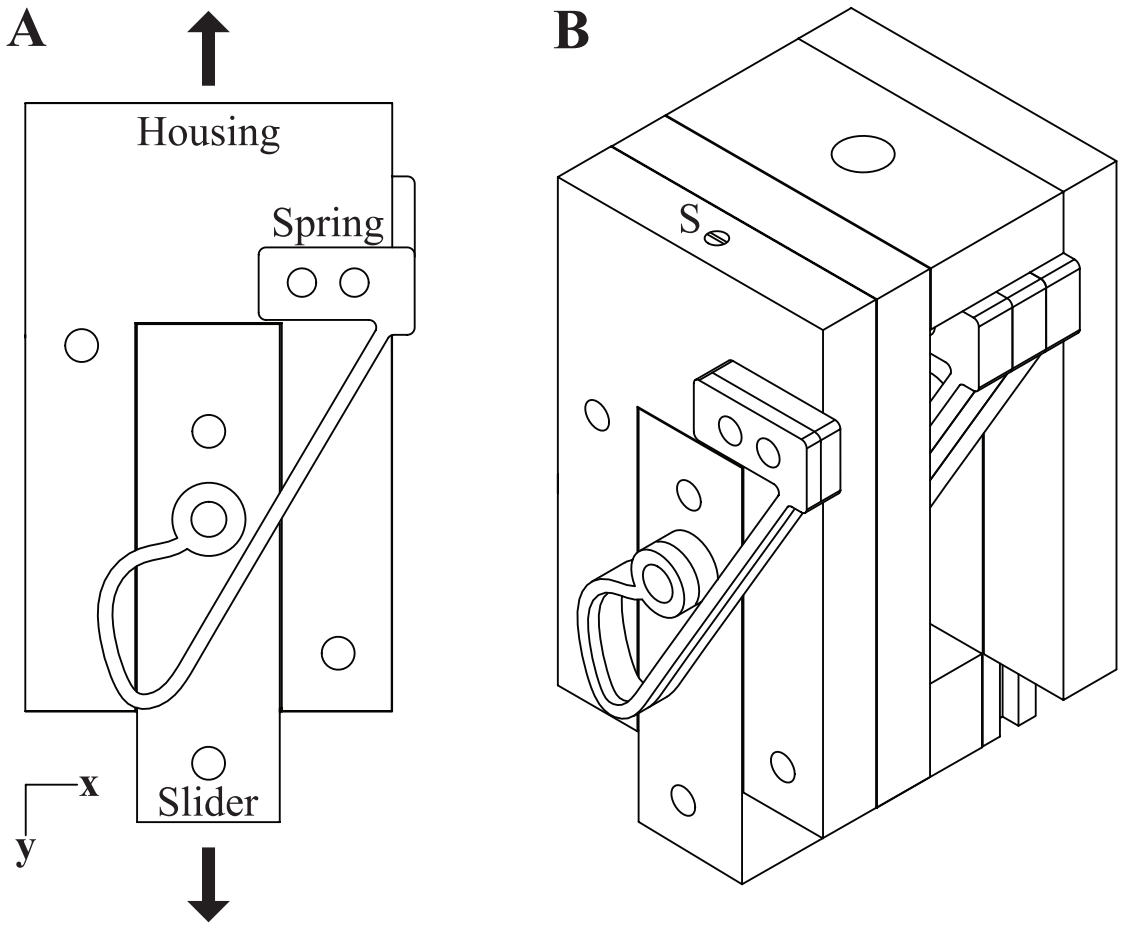

Figure A.1 Diagram of non-linear quadriceps spring housing. (A) Anterior view of the spring and housing. The spring is attached to the slider with a metallic pin, constraining motion to the y-direction only. The arrows show the direction of loading. (B) The spring housing viewed from in a three-quarter lateral view. The three titanium springs comprising the "female spring" can be seen at right. The two supplemental springs and aluminum plate needed to increase the quadriceps tensile stiffness by 20% to male values are show at left. The screw, S, is used to adjust the supplemental spring length to the same length as the female spring. This allows the interchangeable plate to be added or removed without unloading the female spring.

A.4 Results

Sample measured force-displacement relationships for the male and female quadriceps springs are shown in Figure A.2. The female quadriceps spring had an initial stiffness of 155 N/mm, followed by a final stiffness of 27 N/mm. The male quadriceps spring had an initial stiffness of 193 N/mm and a final stiffness of 46 N/mm. The break

point for the bi-linear behavior occurred at approximately 4.5 mm. The male and female quadriceps springs were compared during 2*BW simulated pivot and non-pivot landings in eight females (Figure A.3). The peak quadriceps force was greater during the pivot landing than the non-pivot landings ($p = 0.014$). The male quadriceps spring trended towards greater peak quadriceps force than the female quadriceps spring ($p = 0.103$).

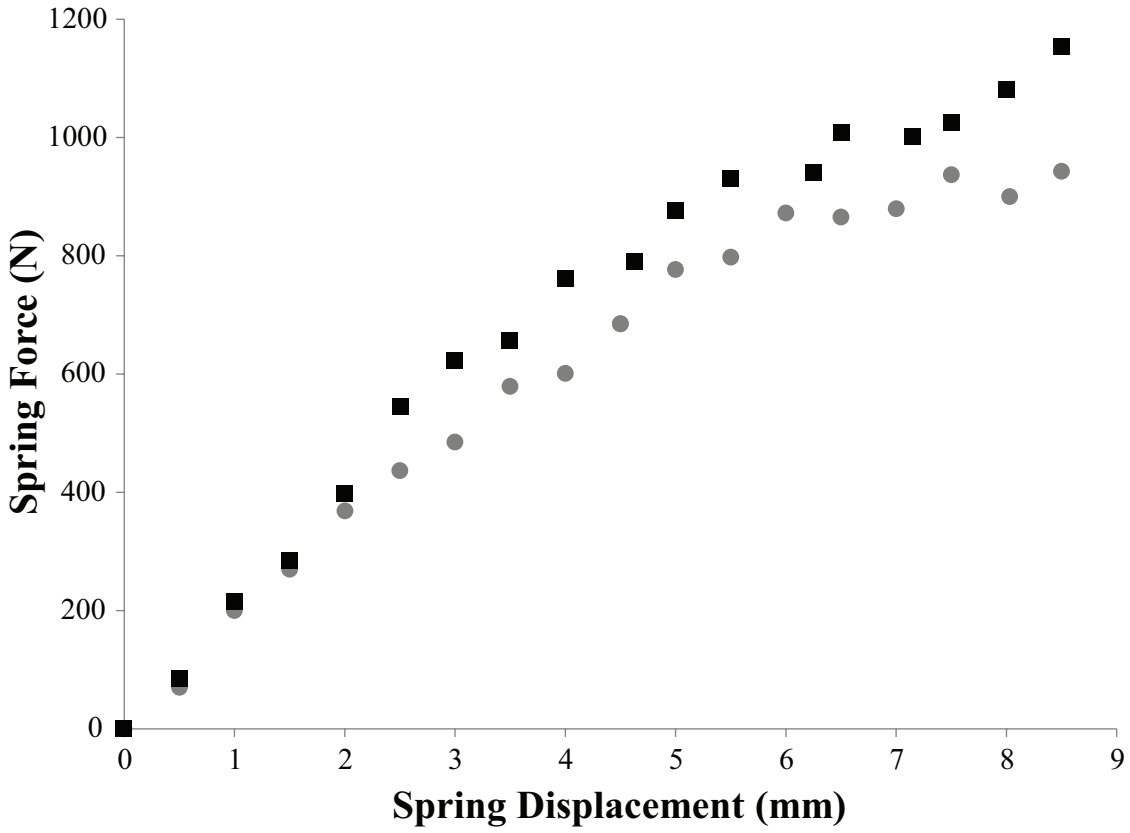

Figure A.2 Sample quasistatic force-displacement relationship for the male (black square) and female (grey circle) non-linear quadriceps spring.

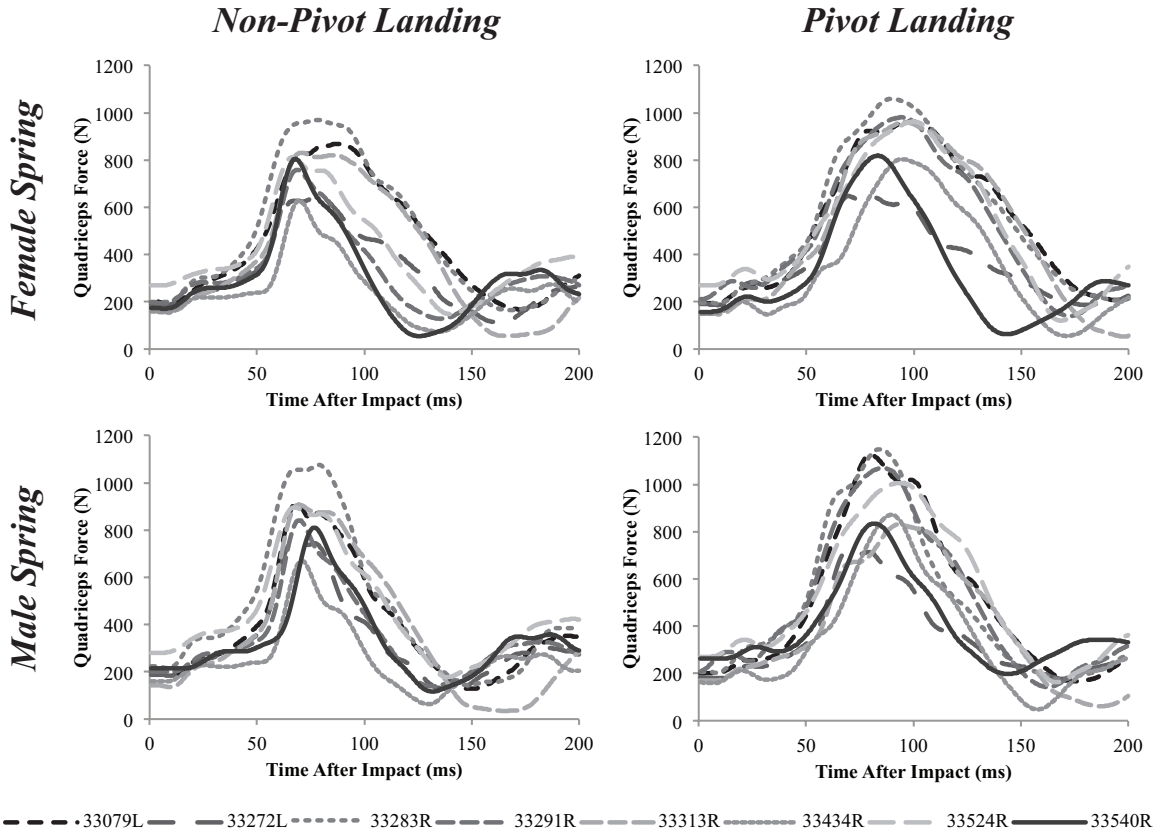

Figure A.3 Quadriceps force-time profiles, each measured in the third trial, from eight female knees undergoing a 2*BW simulated non-pivot and pivot landing with the female and male non-linear quadriceps springs.

A.5 Discussion

A novel, compact non-linear spring unit capable of simulating the active response of the male and female human quadriceps muscle to rapid stretch during the first 100 ms of a jump landing was developed and tested. The peak quadriceps force values achieved during 2*BW pivot and non-pivot simulated landings (Figure A.3) show that the majority of knees imposed quadriceps force levels beyond the spring's force-length breakpoint (Figure A.2). This occurred more often with the pivot landings since peak quadriceps force was significantly greater than during the non-pivot landings. The trend towards greater peak quadriceps force with the male spring was not surprising because the higher

male stiffness will produce a greater force than the female spring for a given displacement.

Active muscle has a non-linear force-length response to rapid stretch that is dependent on the sarcomere length-tension curve[1, 2, 8]. Assuming a vastus lateralis fascicle has 32,500 in-series sarcomeres[4], we estimate the sarcomere length of the vastus lateralis during a drop jump is 2.71 μm to 3.07 μm[7], which places its excursion between the fascicle's optimal length and the top of the descending limb of the force-length curve. Single muscle fibers show a high initial stiffness up to a yield point, followed by no force enhancement for muscle fibers near their optimal length and residual force enhancement for muscle fibers on the descending limb. The residual force enhancement is due to the parallel elastic elements, like titan, increasing supporting regions with small filament overlap allowing the areas of greater filament overlap to continue to increase the force output of the muscle[3]. Indeed, the *in vivo* behavior of the human quadriceps muscle exhibits residual force enhancement[18].

The active stretch response of single fibers is also stretch-rate dependent, as shown in type II muscle fibers[12] and whole muscle[6]. Active whole muscle stretch at 2.5 or 10 cm/s shows a similar response to rapid stretch as single muscle fibers. However, if whole muscle is stretched above 25 cm/s, there will be a force decrement beyond the yield point. Assuming a vastus lateralis fascicle length of 88 mm[4], and that the vastus lateralis will stretch 20 mm in the first 100 ms following initial contact during a drop jump[7], we estimate the quadriceps stretch rate is 2.3 fiber lengths per second during the initial phase of a jump landing. This is well within the *in vivo* stretch rate range that exhibits a bi-linear force-displacement response[6, 12].

These non-linear quadriceps springs significantly improve upon existing methods of simulating lengthening muscle forces during dynamic *in vitro* simulations of musculoskeletal behavior. Previous studies have modeled muscle forces dynamically using linear springs[14, 20], quasi-statically by placing muscle force at a pre-set value[19], or have ignored muscle forces[13]. Current theoretical models predicting quadriceps forces during a jump landing are predicated upon Hill-type models (for example,[15], which concern shortening muscle behavior; this unfortunately means that they cannot be validated against our measured quadriceps force-time relationships (Figure A.3). Our non-linear springs are limited in the range of forces developed for a given excursion. The current non-linear springs were optimized to represent quadriceps force during a 2*BW landing. For larger loadings, the spring's load-displacement behavior will need to be adjusted to properly model the bi-linear behavior.

A.6 Conclusions

The novel gender-specific design of these non-linear quadriceps springs exhibited the desired bilinear tensile force-displacement behaviors of the intact adult male and female human quadriceps muscles during the first 100 ms of a simulated pivot landing.

A.7 References

1. Edman KA, Elzinga G, Noble MI. Enhancement of mechanical performance by stretch during tetanic contractions of vertebrate skeletal muscle fibres. *J Physiol.* 1978;281:139-155.

2. Edman KA, Elzinga G, Noble MI. Residual force enhancement after stretch of contracting frog single muscle fibers. *J Gen Physiol.* 1982;80(5):769-784.

3. Edman KA, Tsuchiya T. Strain of passive elements during force enhancement by stretch in frog muscle fibres. *J Physiol.* 1996;490 (Pt 1):191-205.

4. Fukunaga T, Kawakami Y, Kubo K, Kanehisa H. Muscle and tendon interaction during human movements. *Exerc Sport Sci Rev.* 2002;30(3):106-110.

5. Granata KP, Wilson SE, Padua DA. Gender differences in active musculoskeletal stiffness. Part I. Quantification in controlled measurements of knee joint dynamics. *J Electromyogr Kinesiol.* 2002;12(2):119-126.
6. Grover JP, Corr DT, Toumi H, et al. The effect of stretch rate and activation state on skeletal muscle force in the anatomical range. *Clin Biomech (Bristol, Avon).* 2007;22(3):360-368.
7. Ishikawa M, Komi PV. Effects of different dropping intensities on fascicle and tendinous tissue behavior during stretch-shortening cycle exercise. *J Appl Physiol.* 2004;96(3):848-852.
8. Julian FJ, Morgan DL. The effect on tension of non-uniform distribution of length changes applied to frog muscle fibres. *J Physiol.* 1979;293:379-392.
9. Jutte CV, Kota S. Design of nonlinear springs for prescribed load-displacement functions. *Journal of Mechanical Design.* 2008;130(8), 011003.
10. Jutte CV, Kota S. Design of Single, Multiple, and Scaled Nonlinear Springs for Prescribed Nonlinear Responses. *Journal of Mechanical Design.* 2010;132(1), 081403.
11. Lipps DB, Oh YK, Ashton-Miller JA, Wojtys EM. Morphologic characteristics help explain the gender difference in peak anterior cruciate ligament strain during a simulated pivot landing. *Am J Sports Med.* 2012;40(1):32-40.
12. Malamud JG, Godt RE, Nichols TR. Relationship between short-range stiffness and yielding in type-identified, chemically skinned muscle fibers from the cat triceps surae muscles. *J Neurophysiol.* 1996;76(4):2280-2289.
13. Meyer EG, Haut RC. Anterior cruciate ligament injury induced by internal tibial torsion or tibiofemoral compression. *J Biomech.* 2008;41(16):3377-3383.
14. Oh YK, Lipps DB, Ashton-Miller JA, Wojtys EM. What strains the anterior cruciate ligament during a pivot landing? *Am J Sports Med.* 2012;40(3):574-583.
15. Pflum MA, Shelburne KB, Torry MR, Decker MJ, Pandy MG. Model prediction of anterior cruciate ligament force during drop-landings. *Med Sci Sports Exerc.* 2004;36(11):1949-1958.
16. Pincivero DM, Salfetnikov Y, Campy RM, Coelho AJ. Angle- and gender-specific quadriceps femoris muscle recruitment and knee extensor torque. *J Biomech.* 2004;37(11):1689-1697.
17. Russell KA, Palmieri RM, Zinder SM, Ingersoll CD. Sex differences in valgus knee angle during a single-leg drop jump. *J Athl Train.* 2006;41(2):166-171.
18. Shim J, Garner B. Residual force enhancement during voluntary contractions of knee extensors and flexors at short and long muscle lengths. *J Biomech.* 2012;45(6):913-918.
19. Weinhold PS, Stewart JD, Liu HY, Lin CF, Garrett WE, Yu B. The influence of gender-specific loading patterns of the stop-jump task on anterior cruciate ligament strain. *Injury.* 2007;38(8):973-978.
20. Withrow TJ, Huston LJ, Wojtys EM, Ashton-Miller JA. The relationship between quadriceps muscle force, knee flexion, and anterior cruciate ligament strain in an in vitro simulated jump landing. *Am J Sports Med.* 2006;34(2):269-274.

APPENDIX B

MATHEMATICAL PREDICTION OF THE GENDER DIFFERENCE IN PEAK ACL STRAIN BASED ON KNOWN GENDER DIFFERENCES IN ACL CROSS-SECIONAL AREA AND TENSILE MODULI

We assumed that after initial preconditioning an ACL will exhibit predominantly hyperelastic behavior under uniaxial elongation. Using Fung's representation of hyperelasticity[3], we simulated how the gender difference in ACL cross-sectional area data reported in this manuscript and the published gender difference in the moduli of elasticity (Chandrashekar et al.[2]) should combine to affect peak ACL strain for a given tensile load on the ligament.

From equation 10 of Fung's model, we first develop a relationship between the modulus of elasticity (E) and the Lagrangian stress of the ligament (T):

$$E = \frac{dT}{d\lambda} = aT \qquad [1]$$

The shape parameter (a) for both males and females can then be calculated as the quotient of the modulus of elasticity and the Lagrangian stress of the ligament over the linear region of a ligament's stress strain curve. The modulus of elasticity was assumed to be 128 MPa for male knees and 99 MPa for female knees[2]. Since Chandrashekar et al. only reported the stress and strain of the ACL at failure, we assume that the Lagrangian stress of the ligament was 25% of its failure value (26.4 MPa for males and 22.6 MPa for

females). We choose 25% because the strain at failure was 0.28, while strains near 0.07 are more realistic for the linear region[1].

The peak ACL strains (ε) for males and females were converted to stretch ratios (λ) using the following relationship, where * indicates the measurement is taken at a specific point (in this case, where peak ACL strain occurs):

$$\lambda^* = \sqrt{2\varepsilon^* + 1} \qquad [2]$$

The Lagrangian stress of the ligament at peak ACL stress can be determined from the undeformed ACL cross-sectional area (A) reported in our results for males and females and the tensile force (P) placed on the ligament:

$$T^* = \frac{P^*}{A} \qquad [3]$$

The ACL tensile force at peak ACL strain can be estimated as follows. We assume:

- The quadriceps force, shown in Table 2.2, is equal to the patellar force
- The male and female ACL forces will be the same since the knees came from size-matched individuals and there was only a 5% gender difference in measured quadriceps force.
- The knee has an initial knee flexion angle of 15 degrees
- The knee undergoes the knee flexion changes for a simulated pivot landing shown in Table 2.2.

With these assumptions, we estimate the ACL force at peak ACL strain will be 350 N. The Lagrangian stress-stretch ratio curve for male and female ACLs can then be determined from equation 13 of Fung's model and is shown in Figure B.1:

$$T = T^* e^{a(\lambda - \lambda^*)} \qquad [4]$$

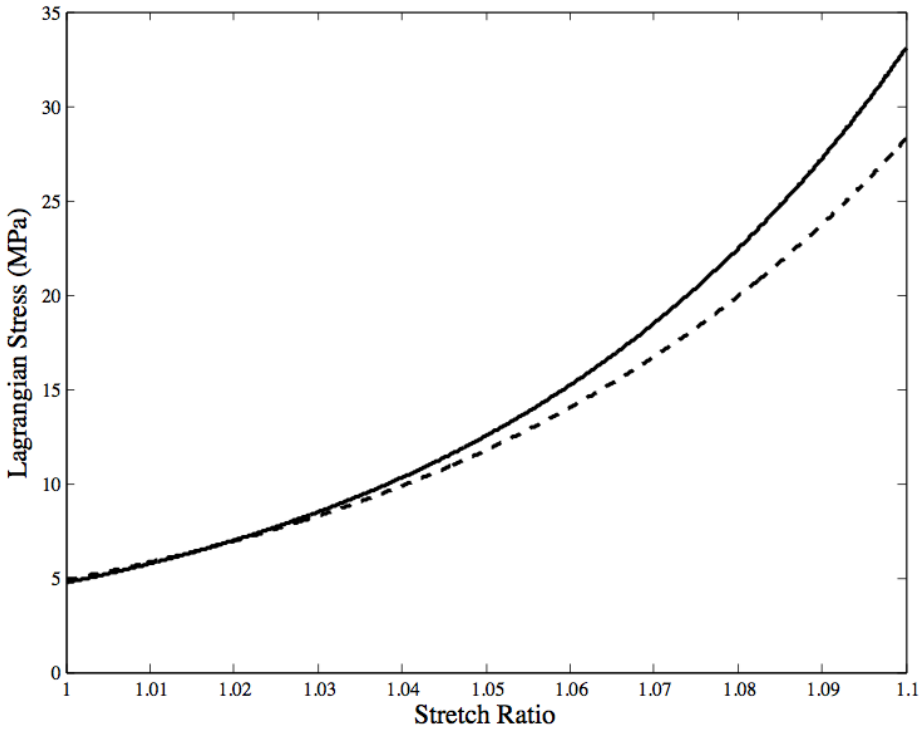

Figure B.1 The Lagrangian stress-stretch curve for male (solid) and female (dashed) ACLs.

From equation [3], we calculate males have a T* value of 8.84 MPa. From Figure A.1, we can determine a stretch ratio of 1.032 which corresponds to a stress of 8.84 MPa. Since females had a 39% smaller ACL cross-sectional area in our study, we would expect females to have a 39% greater stress than males for the same ACL force. For a T* value of 12.29 MPa, females will have a stretch ratio of 1.053. The female and male stretch ratios can then be expressed as a gender ratio of peak strains:

$$\frac{\varepsilon_F}{\varepsilon_M} = \frac{\lambda_F^2 - 1}{\lambda_M^2 - 1} \qquad [5]$$

Therefore, our hyperelastic ligament model predicts the strain in the female ACL should be 1.67 times larger than male ACLs. This may be compared to our experimental results which demonstrated a 1.95 fold greater peak ACL strain in the female ACL than

the male ACL. Our hyperelastic model, which considers gender-specific moduli of elasticity and ACL cross-sectional area, therefore predicts about 2/3rds of the observed gender difference in peak ACL strain. Additional gender differences in mechanical and anatomical parameters likely contribute to the overall strain on the ligament, including the posterior tibial slope and femoral notch size, but these were not measured in this study.

References

1. Butler DL, Guan Y, Kay MD, Cummings JF, Feder SM, Levy MS. Location-dependent variations in the material properties of the anterior cruciate ligament. *J Biomech.* 1992;25(5):511-518.
2. Chandrashekar N, Mansouri H, Slauterbeck J, Hashemi J. Sex-based differences in the tensile properties of the human anterior cruciate ligament. *J Biomech.* 2006;39(16):2943-2950.
3. Fung YCB. Elasticity of soft tissues in simple elongation. *Am J Physiol.* 1967;213(6):1532-1544.

APPENDIX C

DESCRIPTION OF DYNAMIC AND QUASI-STATIC BIOMECHANICAL MODELS OF THE KNEE JOINT TO EXPLAIN THE EFFECT OF QUADRICEPS STIFFNESS ON PEAK ACL STRAIN AND KNEE FLEXION

A 3D lower-limb model was constructed using sagittal magnetic resonance (MR) images (T2-weighted, 3D-PD sequence, TR/TE: 1000/35 ms, slice thickness: 0.35 mm, FOV: 160 mm) of a male cadaveric lower-limb[3] (age:47 yrs, weight:778 N, height: 1.85 m). The distal femur, proximal tibia, fibula and patella were segmented (SolidWorks 2010, Dassault Systems SolidWorks Corp., Concord, MA; Rhinoceros, McNeel North America, Seattle, WA) and imported into a dynamic motion simulation software (MD ADAMS R3, MSC. Software, Inc., Santa Ana, CA). As previously described[2,3], eighteen viscoelastic elements were used for the mechanical behavior of the knee joint ligament and capsular structure (Figure C.1). The ligament or capsular force was defined according to Shin et al.'s work[4]. The model improves on the initial dynamic 3D model[3] because of the use of tibial bone morphology, rather than assuming the tibial plateaus are plates. A new feature of this model was the assumption that the interaction between the surfaces of the femur and tibia within the knee joint was not frictionless. Static and dynamic coefficients of friction were assumed to be 0.18 and 0.06, respectively, using *in vivo* articular cartilage coefficients of friction[1]. This 3D biomechanical model was utilized for a dynamic model to investigate the effect of quadriceps tensile stiffness on peak AM-ACL relative strain, as well as a quasi-static model to investigate the effects of large

changes in knee flexion angle on peak AM-ACL relative strain under weight-bearing conditions.

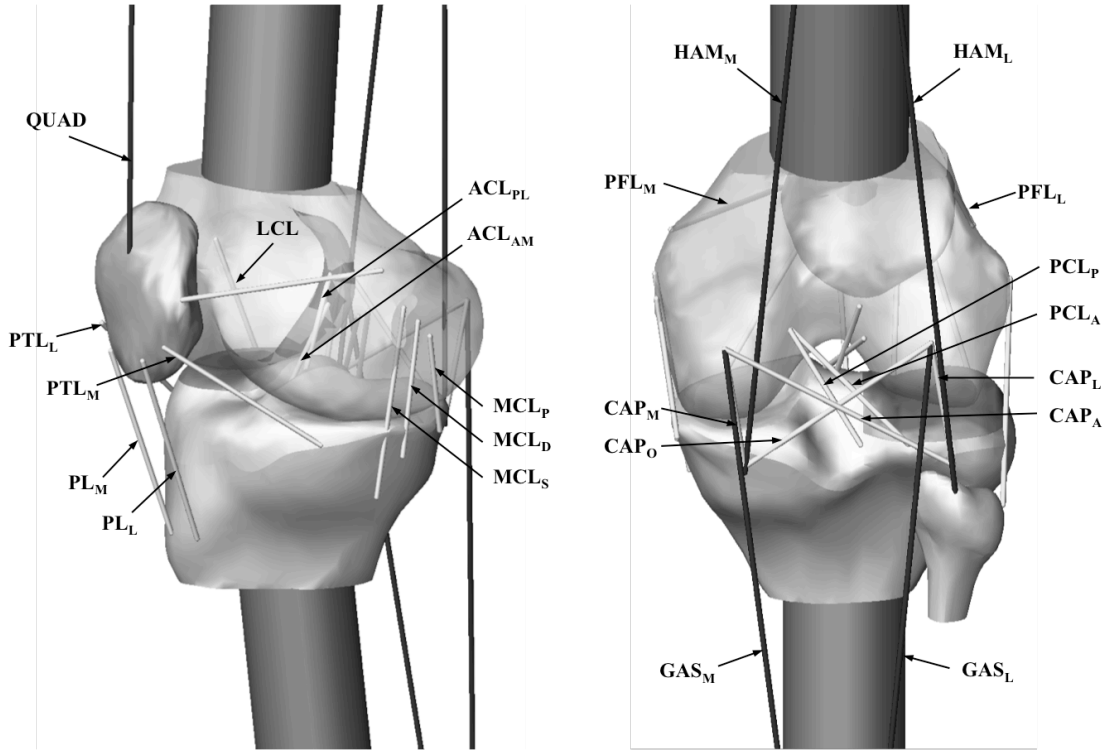

Figure C.1 Schematic of the 3D biomechanical model with femur, tibia, and patella segmented from a human knee with magnetic resonance imaging scan. Ligaments, capsular structures, and muscles are viscoelastically modeled with Kelvin-Voigt elements.

Dynamic In Silico Model

The knee model was built to replicate the experimental set-up (Figure 3.1), where the quadriceps, medial and lateral hamstrings and gastrocnemius muscles were pretensioned to 180 N for quadriceps and 70 N for each flexor muscle, respectively, with the knee initially in 15 degrees of flexion. The impulsive compressive force applied during the experiment drove the simulation. The resultant muscle forces, ACL strain, and kinematics have been previously validated against the *in vitro* experiment results[2,3]. The relative quadriceps tensile stiffness was varied from 70-130 %, with 100% stiffness and

70% stiffness corresponding to the male and female stiffness values utilized during the experiment, respectively. The peak AM-ACL relative strain and peak change in knee flexion angle were monitored over the first 100 ms of the dynamic impact.

As quadriceps tensile stiffness was increased, there was a corresponding decrease in peak AM-ACL relative strain and knee flexion angle (Figure 3.4). There appears to be a relationship between how much the femur rolls relative to the tibial plateau and how much the ACL is strained, confirming the experimental results (Figure 3.3). As the femur rolls posteriorly, the initial femoral contact point will slide anteriorly relative to the initial tibial contact point, but the absolute femoral translation will move posterior to the tibial plateau, increasing ACL strain. In order to investigate this phenomenon further, a second quasi-static model is needed.

Quasi-Static In Silico Model

Using the same 3D biomechanical model, a kinematic-based quasi-static model was developed where the quadriceps force was held constant (ranging from 600 – 1,400 N). Rather than using the dynamic experimental forces to drive the model, the proximal tibia was pushed proximally (i.e., upwards from the ground) in order to change the knee flexion angle from 0 – 25 degrees, relative to the starting knee flexion angle of 12 degrees. The resultant changes in AM-ACL relative strain were monitored.

The AM-ACL relative strain will increase over the initial 5 – 6 degree change in knee flexion angle since the femur is primarily rolling (Figure C.2). Additional knee flexion, and therefore additional rolling, will eventually cause AM-ACL relative strain to decrease. As the knee continues to flex, the AM-ACL relative strain will begin to decrease as the initial femoral contact point begins to slide anterior to the initial tibial

contact point while rolling (Note: the absolute translation of the femur relative to the tibial plateau will continue to move posteriorly as the knee flexes over the full range of the model). The amount of quadriceps force does not seem to affect this trend, and instead only modulates the level of ACL strain. While landing with a greater change in knee flexion can reduce ACL strain, we cannot ignore the possibility that initial femoral rolling before any significant femoral sliding begins may be the most damaging situation to the ACL in a knee near full extension. Since the experimental results show reduced muscle capacity (i.e., less quadriceps tensile stiffness) enhances ACL strain, females may be more prone to ACL injuries especially since the injury typically occurs in the first 100 ms following initial ground contact.

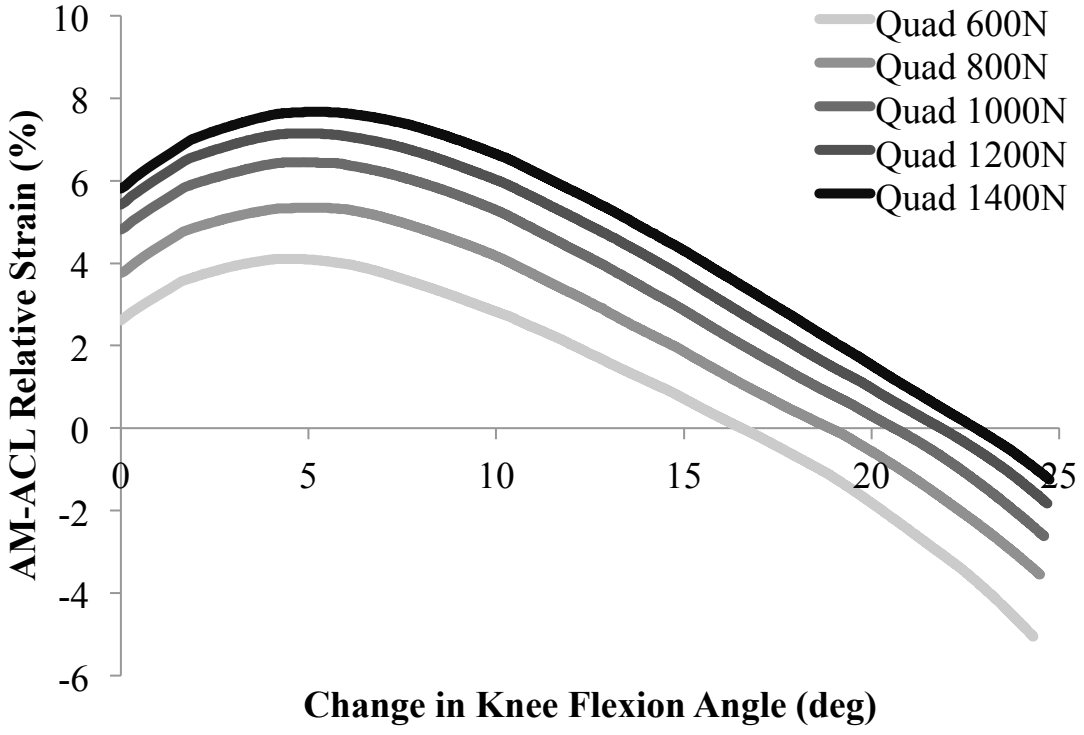

Figure C.2 The effect of an increasing change in knee flexion angle (relative to an initial angle of 12 degrees) on AM-ACL relative strain. Results are from a quasi-static biomechanical model of the knee joint utilizing varying levels of constant quadriceps force.

Model Limitations

The main limitation of the *in silico* biomechanical model presented in this appendix is the value of the friction coefficients. While the authors did their best to match the model to *in vivo* static and dynamic coefficients of friction, major changes in these variables could affect the model results. Other limitations of this biomechanical model have been discussed previously [2,3].

References

1. McCann L, Ingham E, Jin Z, Fisher J. Influence of the meniscus on friction and degradation of cartilage in the natural knee joint. *Osteoarthritis and Cartilage*. 2009; 17:995-1000.
2. Oh YK, Lipps DB, Ashton-Miller JA, Wojtys EM. What strains the anterior cruciate ligament during a pivot landing? *Am J Sports Med.* 2011. (in press)
3. Oh YK. On the mechanism of non-contact ACL injuries during a simulated jump landing: Experimental and theoretical analyses [dissertation]. Ann Arbor: University of Michigan-Ann Arbor; 2011.
4. Shin CS, Chaudhari AM, Andriacchi TP. The influence of deceleration forces on ACL strain during single-leg landing: A simulation study. *J Biomech.* 2007;40(5):1145-1152.

APPENDIX D

A PHOTOGRAPHIC REVIEW OF ANTERIOR CRUCIATE LIGAMENT FATIGUE FAILURES DURING SIMULATED PIVOT LANDINGS

The following appendix highlights the different types of ACL fatigue failures produced in Chapter 4 with a 3 to 5 body-weight (BW) simulated pivot landing. Following the fatigue failure protocol, all 20 knees (10 matched-pairs, 5 male) were visually inspected for damage with the knee joint flexed to ~135° and the rectus femoris tendon moved distally to provide a clear view of the ACL within the knee joint. All photographs were shot from a distal view of the femoral condyles, providing an anterior view of the ACL within the femoral intercondylar notch. No photographs were taken of from a posterior view of the ACL. The photographs were taken with a 14.1 megapixel camera (Canon Powershot SD1400IS, Toyko, Japan). Images were retouched in Adobe Photoshop (CS5.1, San Jose, CA) to simplify the background surrounding the knee joint. The type and location of the fatigue failure were classified from the visual inspection. The type of fatigue failures included complete ACL tears (> 75% damage), partial ACL tears, tibial avulsions, and no injury. In addition, a fifth category of fatigue failure was determined from testing data: if there was a 3-mm increase in absolute anterior tibial translation during testing, the ligament was classified as permanent elongation. The permanent elongated ligaments did not show visual signs of tearing to the human eye, but the ligament fibers often showed a wavy pattern. The location of the fatigue failures was defined as the bundle injured (posterolateral or anteromedial) and whether the injury

occurred mid-substance or near the femoral or tibial insertions of the ACL. Each matched-pair donor is presented in a panel of two images, with the left and right panel showing the fatigue failure damage to the corresponding knee.

Donor #32381: 54 year old male

The left knee of Donor #32381 underwent an average 3.6 BW simulated pivot landing with a 32.3 Nm internal tibial torque, while the right knee underwent an average 4.5 BW simulated pivot landing with 43.2 Nm internal tibial torque. The left knee did not show macroscopic tearing (Figure D.1, left). However, there does appear to be more waviness in the posterolateral bundle when compared to the anteromedial bundle, and there was a 3-mm increase in absolute anterior tibial translation after 48 cycles. The right knee shows a partial tear of the posterolateral bundle near the femoral insertion (Figure D.1 right), which was ruptured after 6 trials.

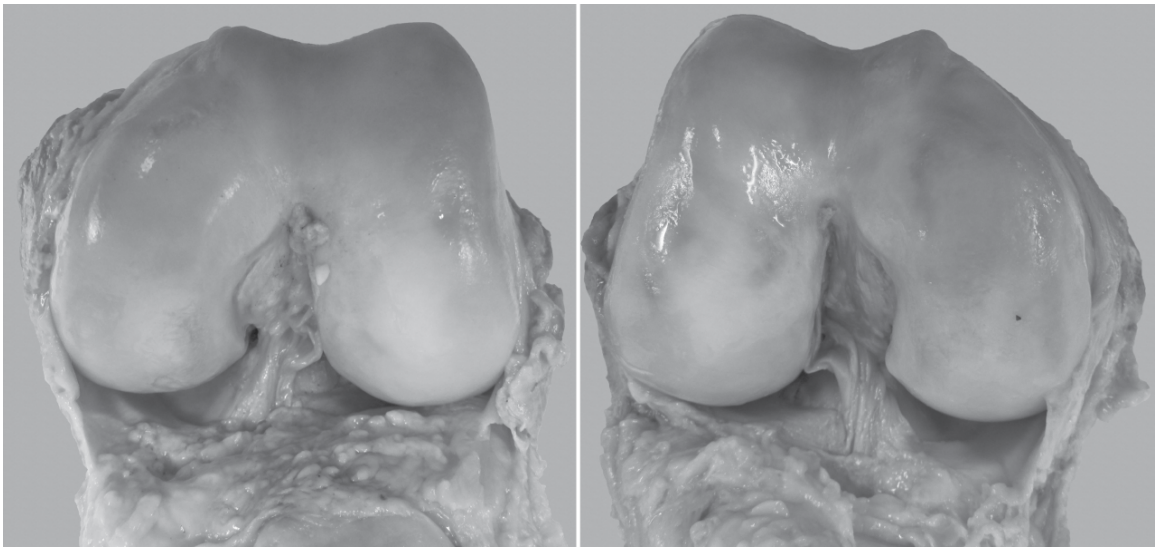

Figure D.1 The left knee of Donor #32381 underwent permanent elongation, while the right knee showed a partial tear of the posterolateral bundle near the femoral insertion.

Donor #61535: 59 year old male

There was no macroscopic damage to the ACL of either knee from Donor #61535 (Figure D.2). The left knee underwent repetitive 4.8 BW simulated pivot landing with 39.2 Nm internal tibial torque and right knee underwent repetitive 3.9 BW simulated pivot landings with 33.2 Nm internal tibial torque for 65 total trials.

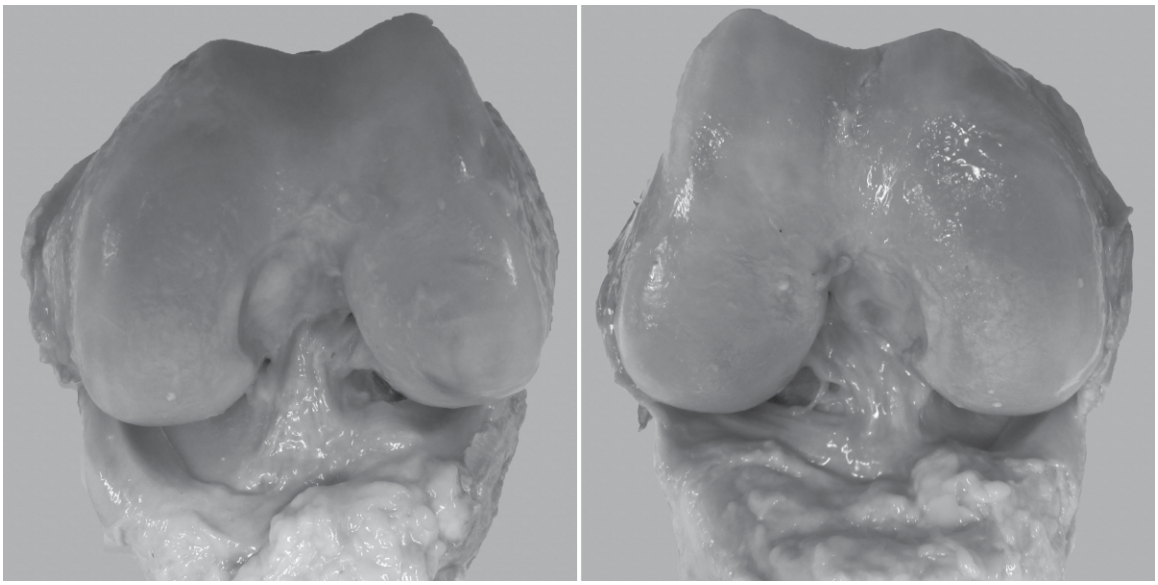

Figure D.2 The left and right knees of Donor #61535 showed no macroscopic tearing of the ACL following the fatigue failure protocol for 65 trials.

Donor #33449: 40 year old male

The left knee of Donor #34449 showed no macroscopic tearing of the ACL following 100 trials of an average 3.8 BW simulated pivot landing with 38.8 Nm internal tibial torque (Figure D.3, left). While the right knee did not show macroscopic tearing, there was a 3-mm increase in absolute anterior tibial translation following 52 trials of an average 4.7 BW simulated pivot landing with 42.7 Nm internal tibial torque (Figure D.3, right). When comparing the two images, the right ACL does appear to have undergone more damage than the left ACL.

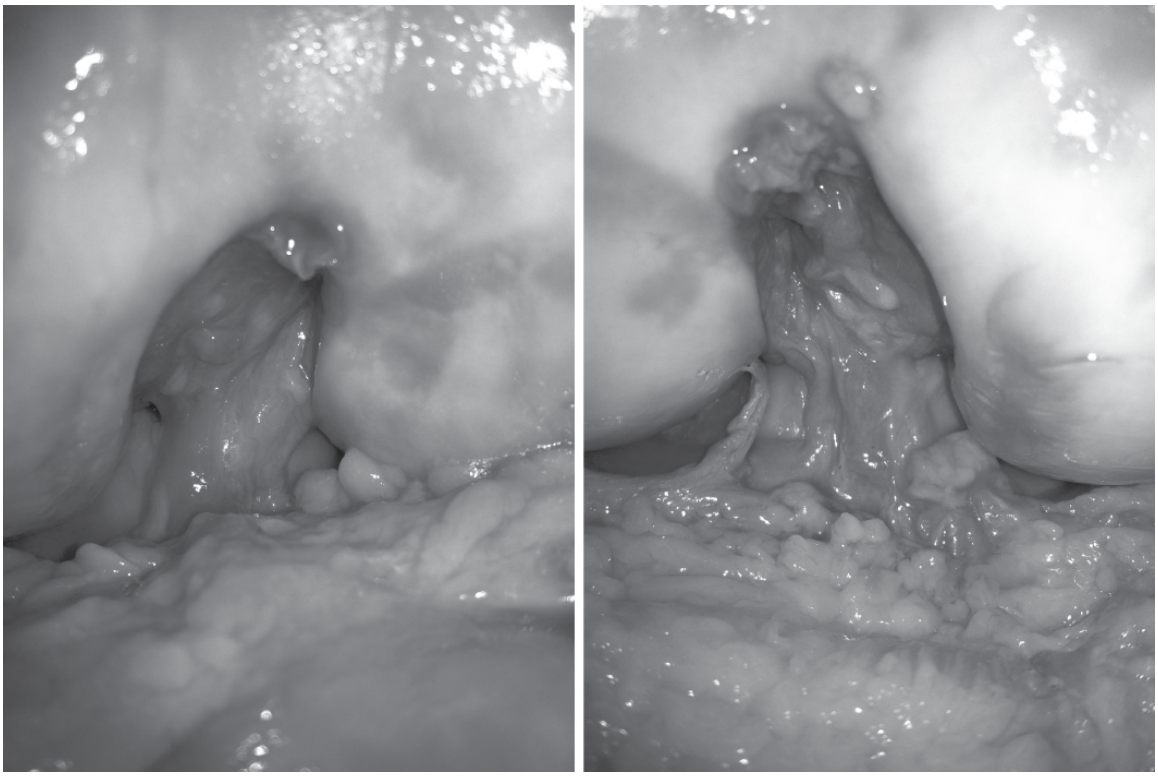

Figure D.3 The left knee of Donor #33449 showed no macroscopic ACL damage, while the right knee underwent permanent ACL elongation.

Donor #33812: 58 year old male

The left knee of donor #33812 suffered a tibial avulsion of the ACL following 8 trials of a 4.1 BW simulated pivot landing with a 34 Nm internal tibial torque (Figure D.4, left). The right knee showed a partial tear on each ACL bundle following 46 trials of an average 3.6 BW with a 30.6 Nm internal tibial torque (Figure D.4, right). The posterolateral ACL bundle showed a partial tear near the femoral insertion, while the anteromedial ACL bundle showed a partial tear near the tibial origin.

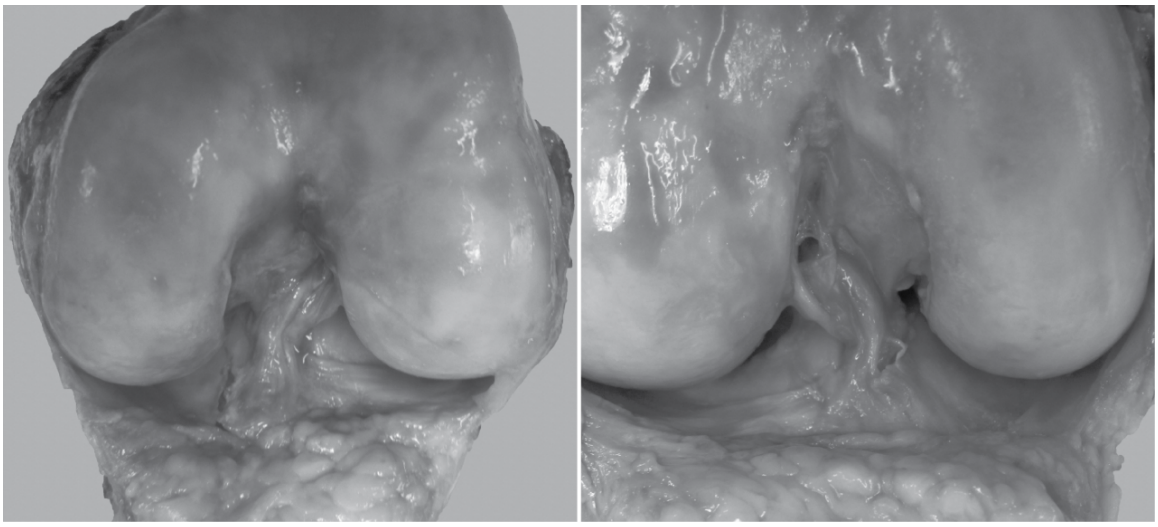

Figure D.4 The left knee of Donor #33812 shows a tibial avulsion of the ACL, while the right knee shows a pair of partial tears to the posterolateral ACL bundle near the femoral insertion and the anteromedial ACL bundle near the tibial origin.

Donor #72780: 52 year old male

The left and right knees of Donor #72780 showed no visual signs of macroscopic ACL tearing following 80 cycles. The left knee underwent an average 3.9 BW simulated pivot landing with 43.1 Nm internal tibial torque, while the right knee underwent a 3.1 Nm simulated pivot landing with 36.5 Nm internal tibial torque.

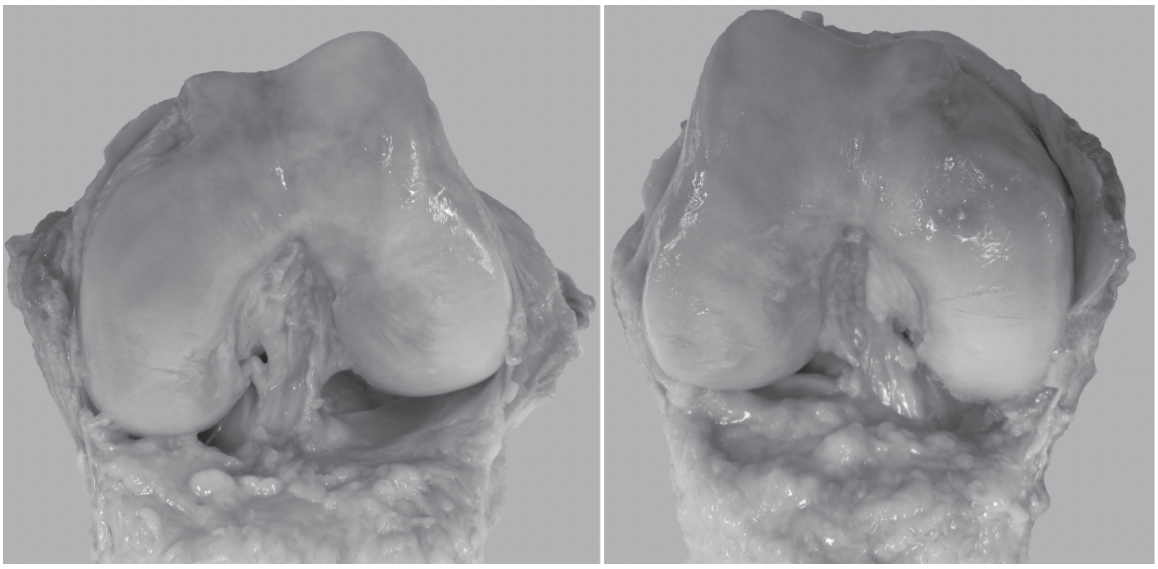

Figure D.5 The left and right knees of Donor #72780 showed no macroscopic ACL tearing.

Donor #42263: 46 year old female

The left knee of Donor #42263 underwent a 3-mm absolute increase in anterior tibial translation following 60 trials of a 3.5 BW simulated pivot landing with 25.9 Nm internal tibial torque. However, there were no signs of macroscopic ACL tearing (Figure D.6, left). The right knee also showed a 3-mm increase in absolute anterior tibial translation following 34 trials of a 4.6 BW simulated pivot landing with 28.1 Nm internal tibial torque. The ACL was classified as having a partial ACL tear of the posterolateral bundle near the femoral insertion.

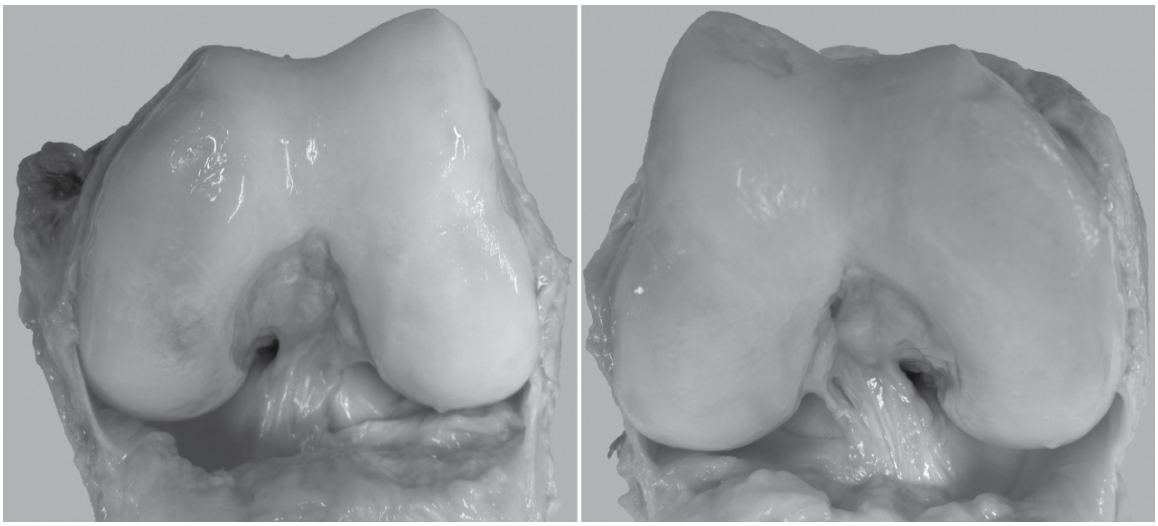

Figure D.6 The left knee of Donor #42263 was permanent elongated, with the right knee showed partial tearing of the posterolateral bundle near the femoral insertion combined with permanent elongation.

Donor #33913: 59 year old female

The left and right knees of Donor #33913 both suffered partial ACL tears of the posterolateral bundle near the femoral insertion (Figure D.7). The left knee failed in 7 cycles under an average 4.2 BW simulated pivot landing with 23 Nm internal tibial torque, while the right knee failed in 17 cycles under an average 3.4 BW simulated pivot landing with 22.6 Nm internal tibial torque.

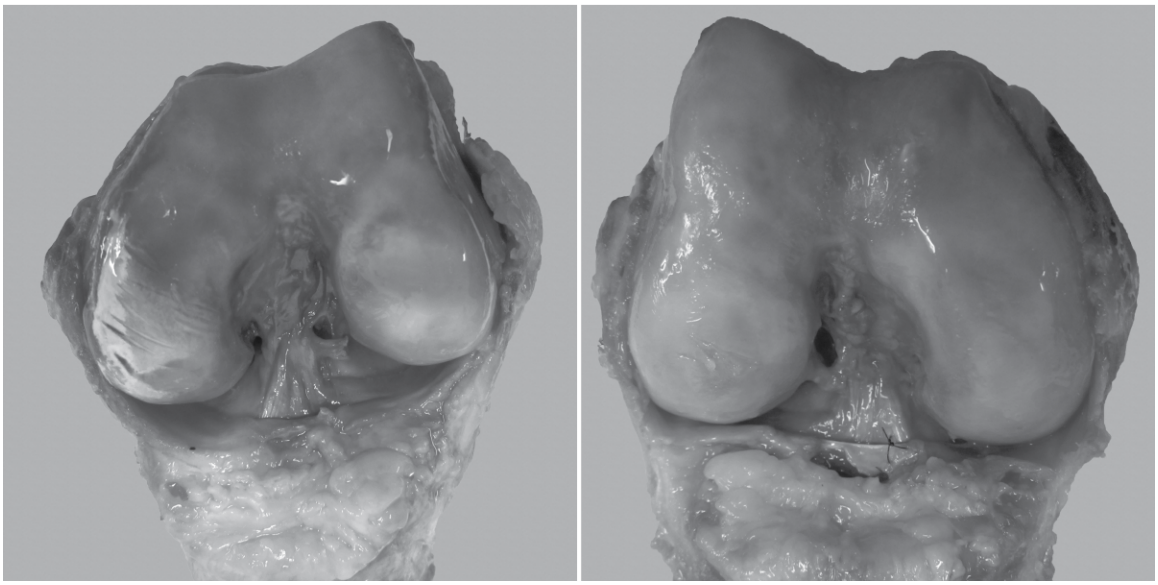

Figure D.7 The left and right knees of Donor #33913 had partial ACL tears of the posterolateral bundle near the femoral insertion.

Donor #34015: 48 year old female

The left knee of Donor #34015 did not show macroscopic ACL tearing following 90 cycles of an average 3.3 BW simulated pivot landing with 24.3 Nm internal tibial torque (Figure D.8, left). While the left knee did not reach a 3-mm increase in absolute anterior tibial translation, there was a clear waviness to the posterolateral bundles upon visual inspection. The right knee had a partial mid-substance ACL tear of the posterolateral bundle following 18 trials of an average 4.1 BW simulated pivot landing with 27.6 Nm internal tibial torque (Figure D.8, right).

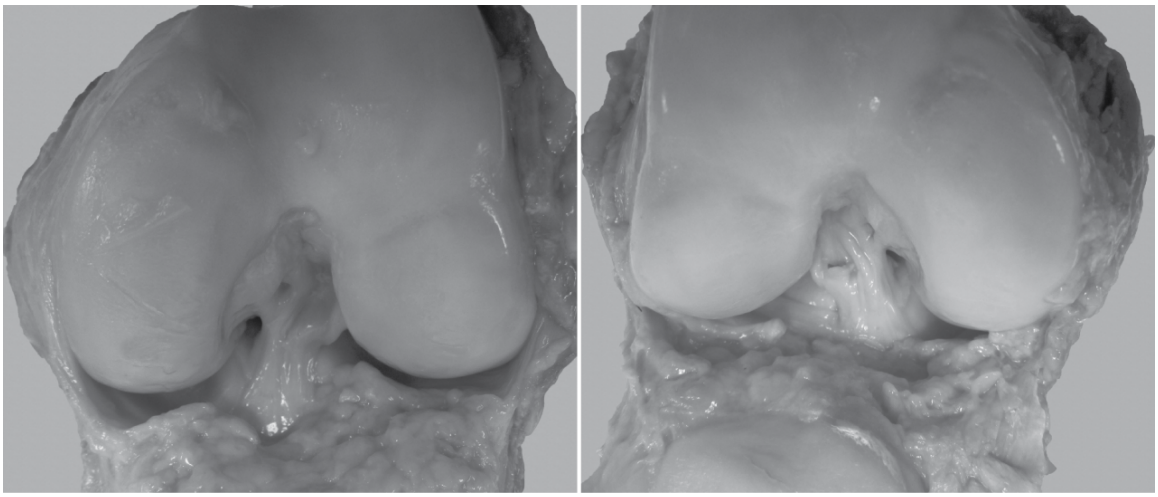

Figure D.8 The left knee of Donor #34015 did not show macroscopic ACL tearing, while the right knee had a mid-substance partial ACL tear of the posterolateral bundle.

Donor #11442: 55 year old female

The left knee of Donor #11442 had a complete ACL tear, with greater than 75% of the ligament showing macroscopic damage (Figure D.9, left). This complete ACL tear occurred after 7 cycles of an average 3.8 BW simulated pivot landings with 34 Nm internal tibial torque. The right knee underwent a 3-mm increase in absolute anterior tibial translation after 66 cycles of an average 3.1 BW simulated pivot landings with 28.3 Nm internal tibial torque. The right knee did show some superficial mid-substance damage (Figure D.9, right).

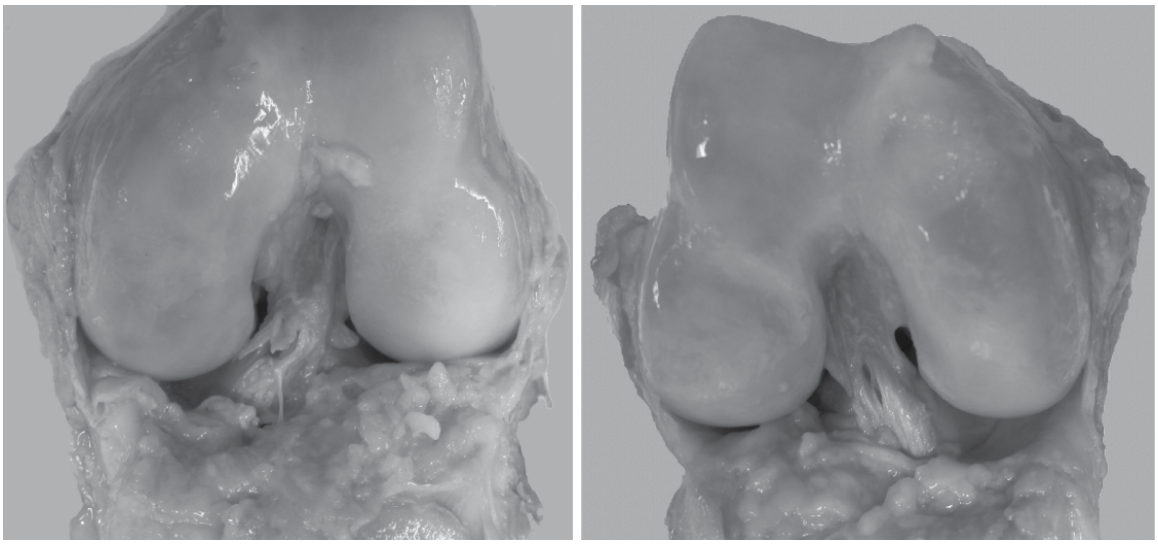

Figure D.9 The left knee of Donor #11442 had a complete ACL tear mid-substance while the right knee was permanent elongated with superficial mid-substance damage.

Donor #34090: 63 year old female

The left knee of Donor #34090 had a tibial avulsion of the ACL following 22 cycles of an average 4.0 BW simulated pivot landing with 29.8 Nm internal tibial torque (Figure D.10, left). There was no macroscopic ACL damage to the right knee following 80 cycles of an average 3.2 BW simulated pivot landing with 25.9 Nm internal tibial torque (Figure D.10, right)

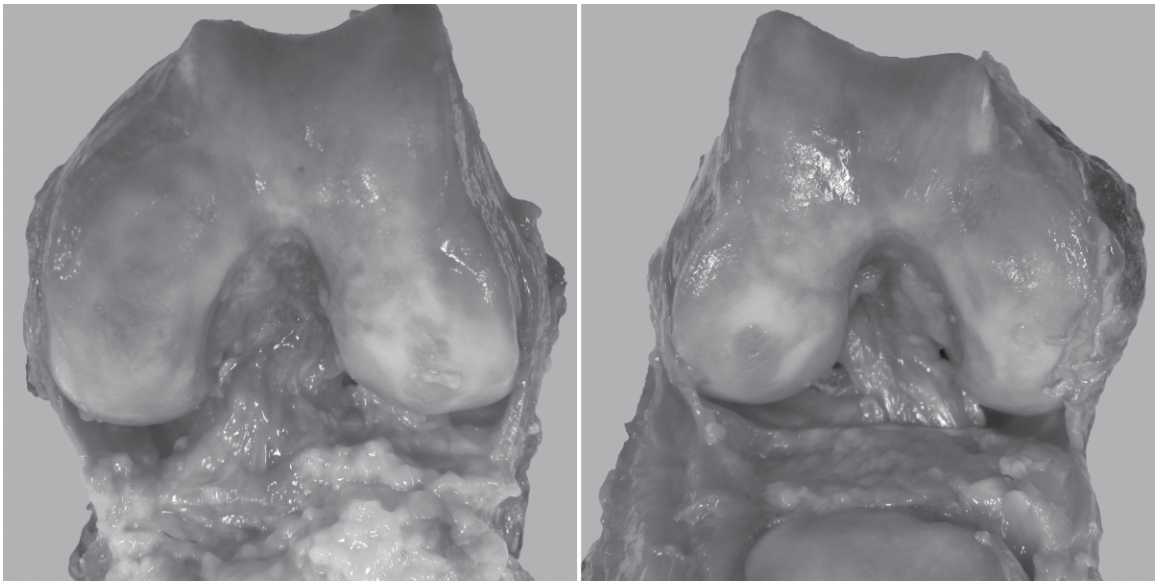

Figure D.10 The left knee of Donor #34090 had a tibial ACL avulsion while the right knee did not show macroscopic ACL damage.

APPENDIX E

COMPREHENSIVE DATASETS FOR THE DISSERTATION

E.1 Overview

This appendix contains the data sets used for the statistical analyses within this dissertation. Donor information and testing data for the pre-baseline, simulated pivot landing, and post-baseline trials for Chapter 2 are shown in Tables E.1 – E.4. Donor information and testing data for pre-baseline, simulated pivot landings with the normal and enhanced female quadriceps tensile stiffness, and post-baseline trials are shown in Tables E.5 – E.9. Donor information and testing data for the final non-pivot, first pivot, failure, and final pivot trials for Chapter 4 are shown in Tables E.10 – E.14. The lateral tibial slope measurements using three different methods by the main observer in Chapter 5 are shown in Tables E.15 – Tables E.16. Finally, the secondary analysis dataset for Chapter 6 is shown in Table E.17.

Table E.1 Donor information and morphologic characteristics for Chapter 2

Donor ID	Age (yrs)	Height (cm)	Mass (kg)	Morphologic Characteristics				
				ACL Cross-Sectional Area (mm^2)	Lateral Tibial Slope (deg)	Medial Tibial Slope (deg)	Medial Tibial Depth (mm)	Bicondylar Width (mm)
M32820R	80	175.3	63.4	42.9	2.7	3.0	2.6	74.5
M32901R	83	167.6	68.0	27.5	5.0	8.4	3.1	65.2
M33105L	53	172.7	68.0					
M33105R	60	165.1	77.0	31.8	4.8	2.6	2.1	74.6
M33160R	84	175.3	68.0	41.5	3.6	6.5	0.7	76.0
M33400L	90	172.7	65.7	37	1.4	4.4	3.2	75.5
M33538R	55	172.7	65.7	33.2	5.4	-1.1	2.4	76.4
M33606L	30	167.6	72.0	40.3	5.4	6.3	2.4	69.5
M33614L	63	172.7	77.0	48.1	3.2	3.4	3.6	76.7
M33610L	59	172.7	63.4	26.9	5.9	4.0	2.5	75.8
F33272L	58	175.3	70.2	22.4	6.7	5.2	1.2	77.3
F33283R	47	193.0	63.4	16.7	6.1	2.3	2.3	69.7
F33291R	75	170.2	68.9	20.2	5.4	6.5	2.3	67.8
F33462R	75	170.2	68.9	21.7	8.0	5.0	0.8	64.1
F33313R	33	157.5	81.5	25.8	5.7	3.6	1.8	65.9
F33079L	89	170.2	72.5					
F33434R	76	177.8	72.5	21.2	0.8	4.3	0.9	
F33524R	54	167.6	72.5	27.5	9.3	7.7	2.1	67.1
F33540R	54	182.9	79.3	24.7	5.1	2.2	1.0	66.2
F33085L	47	180.3	68.0	27.1	2.6	6.1	1.8	64.3

Table E.2 Dataset for Chapter 2: 2*BW Pre-baseline landing (Block A) with compression and flexion moment

Donor ID	Peak Compression Force (N)	Peak AM-ACL Relative Strain (%)	Peak Change in Knee Flexion (deg)	Peak Anterior Tibial Translation (mm)	Peak Quadriceps Force (N)
M32820R	1396	1.61	5.4	2.1	709
M32901R	1335	3.15	5.2	1.2	965
M33105L	1292	2.7	5.3	0.5	948
M33105R	1367	1.93	4.2	1.5	667
M33160R	1589	1.25	3.2	1.2	650
M33400L	1445	0.01	4.9	3.3	764
M33538R	1487	1.03	3.6	2.3	725
M33606L	1380	1.31	4.9	1.4	846
M33614L	1406	0.33	4.8	1.8	868
M33610L	1465	1.78	4.8	1.5	923
F33272L	1016	7.94	8.6	1.8	660
F33283R	922	7.16	8.8	3.0	964
F33291R	1256	1.97	5.6	1.8	745
F33462R	1443	3.09	4.2	2.0	629
F33313R	1068	2.5	10.0	1.6	828
F33079L	970	1.99	9.5	2.2	869
F33434R	1347	1.71	5.1	2.6	649
F33524R	1209	4.24	7.9	4.7	802
F33540R	1404	2.82	5.4	2.8	794
F33085L	1321	0.52	6.0	2.3	802

Table E.3 Dataset for Chapter 2: 2*BW pivot landing ('Block B') with compression, flexion Moment, and internal tibial torque

Donor ID	Peak Compression Force (N)	Peak Internal Tibial Torque (Nm)	Peak AM-ACL Relative Strain (%)	Peak Change in Knee Flexion (deg)	Peak Anterior Tibial Translation (mm)	Peak Internal Tibial Rotation (deg)	Peak Quadriceps Force (N)
M32820R	928	19.3	2.54	7.1	3.5	10.5	786
M32901R	965	10.7	7.86	5.9	3.6	11.0	919
M33105L	784	15.6	2.83	6.7	1.7	10.1	1044
M33105R	993	14.5	2.41	6.1	3.0	7.2	726
M33160R	666	24.1	4.51	7.4	3.0	14.9	949
M33400L	637	23.2	3.58	7.8	7.6	15.1	1051
M33538R	791	25.1	2.48	5.1	4.5	11.3	881
M33606L	750	24.3	2.35	7.9	2.6	11.4	1027
M33614L	797	17.7	0.72	5.3	2.3	11.8	861
M33610L	832	20.4	3.31	5.7	2.5	12.2	1037
F33272L	817	9.3	8.83	7.8	3.2	12.4	659
F33283R	631	10.3	8.13	8.8	3.1	12.5	1043
F33291R	629	17.2	5.6	10.3	4.5	21.1	987
F33462R	872	20.3	7.89	6.4	4.0	14.5	721
F33313R	648	15.3	4.77	12.2	3.8	17.3	978
F33079L	718	15.5	4.71	11.4	3.9	13.0	965
F33434R	580	20.3	4.96	8.3	3.7	19.8	810
F33524R	590	22.2	9.47	10.6	6.6	19.7	972
F33540R	704	23.4	8.04	4.8	2.8	17.5	821
F33085L	692	22.0	1.27	8.8	4.5	15.5	927

Table E.4 Dataset for Chapter 2: 2*BW Post-baseline landing (Block A') with compression and flexion moment

Donor ID	Peak Compression Force (N)	Peak AM-ACL Relative Strain (%)	Peak Change in Knee Flexion (deg)	Peak Anterior Tibial Translation (mm)	Peak Quadriceps Force (N)
M32820R	1387	1.45	4.9	2.0	592
M32901R	1160	2.61	5.9	1.7	959
M33105L	1124	2.2	5.7	0.9	1027
M33105R	1414	2.22	4.4	1.6	494
M33160R	1572	1.55	3.0	1.3	657
M33400L	1347	0.01	5.5	3.5	864
M33538R	1497	1.7	3.4	2.0	771
M33606L	1314	0.72	5.0	1.3	804
M33614L	1345	0.27	4.6	1.5	844
M33610L	1456	1.55	4.4	1.2	817
F33272L	1064	8.35	8.8	2.2	678
F33283R	908	7.13	8.8	2.8	890
F33291R	1184	3.6	5.9	1.6	792
F33462R	1512	2.75	4.0	1.9	641
F33313R	1125	3.15	9.2	1.2	832
F33079L	934	2.34	10.0	2.5	894
F33434R	1294	1.33	5.1	2.6	654
F33524R	1031	5.3	8.4	5.1	805
F33540R	1383	3.33	5.3	2.3	772
F33085L	1398	0.09	5.3	2.0	768

Table E.5 Donor information and morphologic characteristics for Chapter 3

Donor ID	Age (yrs)	Height (cm)	Mass (kg)	Morphologic Characteristics			
				ACL Cross-Sectional Area (mm^2)	Lateral Tibial Slope (deg)	Medial Tibial Slope (deg)	Notch Width Index
FA266L	52	157.5	68.0	20.5	6.9	7.0	0.219
FA827L	52	165.1	63.5	19.6	7.5	8.6	0.229
F33603L	67	152.4	77.1	32	2.8	-2.4	0.293
F33291L	53	172.7	68.0	29.9	5.8	5.5	0.308
F33283L	83	167.6	68.0	22.7	5.7	1.5	0.232
F33971R	61	170.2	79.4	28	8.1	5.8	0.273
FA660L	48	157.5	71.2	28.9	5.1	5.7	0.257
F33955R	52	160.0	65.8	27.4	2.8	6.6	0.294
F33462L	60	165.1	77.1	26	6.7	6.6	0.286
F33434L	30	167.6	72.1	29.9	4.4	1.7	0.280
F33681R	62	162.6	68.0	25.2	5.4	3.6	0.218
F33272R	80	175.3	63.5	21.5	8.4	4.1	0.221

Table E.6 Dataset for Chapter 3: 2*BW Pre-baseline landing with normal female quadriceps stiffness (Block A) with compression and knee flexion moment

Donor ID	Peak Compression Force (N)	Peak AM-ACL Relative Strain (%)	Peak Change in Knee Flexion (deg)	Peak Anterior Tibial Translation (mm)	Peak Quadriceps Force (N)
FA266L	1249	4.0	6.7	3.0	752
FA827L	1164	1.7	6.9	1.6	693
F33603L	1037	2.0	8.6	1.3	755
F33291L	1037	0.8	7.5	4.5	879
F33283L	1144	2.4	6.3	2.0	813
F33971R	1114	3.9	6.7	2.2	718
FA660L	1023	3.3	8.5	2.2	822
F33955R	1174	0.8	5.6	1.4	671
F33462L	1326	2.3	6.5	3.6	738
F33434L	1040	1.0	8.4	2.2	835
F33681R	1204	1.7	7.5	1.4	760
F33272R	1378	4.2	5.0	2.2	760

Table E.7 Dataset for Chapter 3: 2*BW Simulated pivot landing with normal female quadriceps stiffness (Block B) with compression, knee flexion moment, and internal tibial torque

Donor ID	Peak Compression Force (N)	Peak Internal Tibial Torque (Nm)	Peak AM-ACL Relative Strain (%)	Peak Change in Knee Flexion (deg)	Peak Anterior Tibial Translation (mm)	Peak Internal Tibial Rotation (deg)	Peak Change in Knee Abduction Angle (deg)	Peak Quadriceps Force (N)
FA266L	755	17.7	10.6	8.6	5.8	15.1	3.3	834
FA827L	578	20.1	7.3	10.4	4.9	16.4	7.1	860
F33603L	483	21.8	4.8	14.5	3.9	12.9	6.2	939
F33291L	601	17.9	1.5	8.4	5.9	20.8	3.9	1008
F33283L	513	22.1	7.2	9.8	4.6	15.9	3.7	1020
F33971R	698	19.5	7.9	11.5	4.3	14.8	7.2	887
FA660L	601	19.2	6.2	9.0	2.3	19.5	3.8	918
F33955R	553	18.8	3.4	9.4	3.5	19.0	5.6	843
F33462L	594	23.6	3.5	10.7	6.9	18.0	5.2	917
F33434L	545	22.0	5.2	9.8	2.3	19.6	3.8	968
F33681R	794	16.8	3.1	10.9	3.5	18.5	5.6	964
F33272R	749	21.3	10.7	8.5	4.3	17.2	1.7	928

Table E.8 Dataset for Chapter 3: 2*BW Simulated pivot landing with trained female quadriceps stiffness (i.e. 33% greater stiffness) (Block C) with compression, knee flexion moment, and internal tibial torque

Donor ID	Peak Compression Force (N)	Peak Internal Tibial Torque (Nm)	Peak AM-ACL Relative Strain (%)	Peak Change in Knee Flexion (deg)	Peak Anterior Tibial Translation (mm)	Peak Internal Tibial Rotation (deg)	Peak Change in Knee Abduction Angle (deg)	Peak Quadriceps Force (N)
FA266L	811	17.8	8.7	7.1	6.0	15.3	2.2	915
FA827L	598	21.7	5.8	8.1	6.0	16.2	5.2	964
F33603L	479	24.0	3.0	11.4	5.2	15.4	4.6	1100
F33291L	644	19.6	1.0	8.0	6.7	21.8	3.4	1140
F33283L	545	22.9	7.2	9.6	4.6	16.7	3.7	1118
F33971R	767	21.1	7.3	8.6	4.9	14.9	4.5	1006
FA660L	667	19.8	5.7	5.8	3.1	19.6	2.5	995
F33955R	645	22.0	2.9	5.7	3.6	19.2	3.0	895
F33462L	658	25.1	2.6	8.2	6.2	17.1	4.1	947
F33434L	621	21.9	3.4	7.3	3.1	20.4	2.6	1019
F33681R	669	18.2	2.3	9.0	3.6	18.8	4.0	1161
F33272R	713	20.7	9.9	7.8	4.9	16.9	1.3	1013

Table E.9 Dataset for Chapter 3: 2*BW Post-baseline landing with normal female quadriceps stiffness (Block A') with compression and knee flexion moment

Donor ID	Peak Compression Force (N)	Peak AM-ACL Relative Strain (%)	Peak Change in Knee Flexion (deg)	Peak Anterior Tibial Translation (mm)	Peak Quadriceps Force (N)
FA266L	1280	3.0	5.9	2.8	711
FA827L	1144	1.4	6.8	1.8	692
F33603L	1199	2.1	7.1	1.5	694
F33291L	1035	0.8	7.3	4.3	889
F33283L	1119	2.9	6.5	1.8	819
F33971R	1207	3.3	6.1	1.9	678
FA660L	1000	3.5	8.6	2.0	797
F33955R	1127	1.3	6.0	1.6	665
F33462L	1345	1.6	6.0	3.6	717
F33434L	940	1.3	8.0	2.0	819
F33681R	1030	1.8	8.1	1.6	842
F33272R	1289	4.4	5.2	1.9	779

Table E.10 Donor information, morphologic characteristics, and loading conditions for Chapter 4

Donor ID	Age (yrs)	Height (m)	Weight (kg)	Body Mass Index (kg/m^2)	Knee	Morphology		Loading Conditions	
						ACL Cross-Sectional Area (mm^2)	Lateral Tibial Slope (deg)	Mean Peak Compressive Reaction Force (BW)	Mean Peak Internal Tibial Torque (Nm)
M32381	54	1.83	72.6	21.7	L	37	6.6	3.6	32.3
					R	32	7.5	4.5	43.2
M61535	59	1.73	74.9	25.1	L	34	7.3	4.8	39.2
					R	28	7.3	3.9	33.2
M33449	40	1.88	74.9	21.2	L	59	13.8	3.8	38.8
					R	44	15.8	4.7	42.7
M33812	58	1.79	63.6	20.1	L	30	6.5	4.1	34.0
					R	37	10.6	3.6	30.6
M72780	52	1.83	84.0	25.1	L	43	4.3	3.9	43.1
					R	39	6.7	3.1	36.5
F42263	46	1.60	59.0	23.0	L	26	11.1	3.5	25.9
					R	25	13.2	4.6	28.1
F33913	59	1.68	59.0	21.0	L	28	7.3	4.2	23.0
					R	32	8.2	3.4	22.6
F34015	48	1.65	59.0	21.7	L	37	9.7	3.3	24.3
					R	33	8.3	4.1	27.6
F11442	55	1.73	77.2	25.9	L	30	7.3	3.8	34.0
					R	40	6.9	3.1	28.3
F34090	63	1.70	68.1	23.5	L	32	15.2	4.0	29.8
					R	35	11.8	3.2	25.9

Table E.11 Dataset for Chapter 4: Tibiofemoral kinematics, strain, and quadriceps force for 13 failed knees for ACL failure trial

Donor ID	Leg Type	Failure Type	Trials to Failure	Peak Cumulative Anterior Tibial Translation (mm)	Peak Relative Anterior Tibial Translation (mm)	Peak Cumulative Internal Tibial Rotation (deg)	Peak Relative Internal Tibial Rotation (deg)	Peak AM-ACL Cumulative Strain (%)	Peak AM-ACL Relative Strain (%)	Peak Quadriceps Force (N)
M32381	L	E	49	9.5	7.4	16.5	14.2	20.1	12.4	1487
M32381	R	P	6	8.8	8.5	17.4	16.5	23.0	17.0	1863
M33449	R	E	52	11.4	10.0	23.1	18.3	8.2	11.0	1921
M33812	L	A	8	11.9	9.4	22.1	18.9	16.3	8.4	1629
M33812	R	P	46	11.5	8.9	18.4	18.4	11.2	3.6	1772
F42263	L	E	60	12.8	10.1	21.3	17.3	7.7	6.5	1572
F42263	R	P	13	11.4	8.8	22.6	19.2	1.3	3.9	2353
F33913	L	P	7	14.0	13.0	24.6	21.3	38.7	44.7	1564
F33913	R	P	17	8.4	7.5	19.9	17.2	5.1	1.2	1671
F34015	R	P	18	6.4	6.7	19.3	19.0	48.9	9.3	1574
F11442	L	T	7	15.9	15.8	29.1	27.6	28.2	26.5	1602
F11442	R	E	66	7.9	6.1	25.2	20.8	15.2	2.5	1781
F34090	L	A	22	11.5	9.2	17.8	16.2	0.2	7.1	1643

Abbreviations: T – Complete ACL tear; P – Partial ACL tear; A – Tibial ACL avulsion; P – Permanent elongation (i.e. 3-mm increase in cumulative anterior tibial translation)

Table E.12 Dataset for Chapter 4: Tibiofemoral kinematics and strain for 20 knees for final tested trial

Donor ID	Leg Type	Final Trial #	Peak Cumulative Anterior Tibial Translation (mm)	Peak Relative Anterior Tibial Translation (mm)	Peak Cumulative Internal Tibial Rotation (deg)	Peak Relative Internal Tibial Rotation (deg)	Peak AM-ACL Cumulative Strain (%)	Peak AM-ACL Relative Strain (%)	Peak Quadriceps Force (N)
32381	L	80	10.2	8.4	18.3	16.2	25.6	15.6	1685
	R	20	9.0	8.4	17.7	16.1	28.6	22.9	1857
61535	L	55	8.5	6.8	22.0	18.0	3.5	3.0	2169
	R	55	6.0	4.2	22.0	17.1	12.3	3.0	1598
33449	L	100	9.3	8.4	22.7	19.2	8.1	2.1	1454
	R	100	13.8	8.9	24.1	19.6	9.6	9.3	1801
33812	L	9	16.4	11.6	23.9	18.2	9.6	0.0	1622
	R	70	12.3	9.2	16.8	16.8	26.2	2.6	1779
72780	L	80	8.0	6.6	18.7	18.2	5.7	5.1	1876
	R	80	9.0	7.6	20.9	18.5	12.4	7.6	1304
42263	L	80	6.0	5.9	18.1	17.5	-0.3	6.9	1503
	R	55	11.7	9.9	23.2	21.1	-5.8	0.9	2578
33913	L	13	14.0	13.0	24.6	21.3	38.7	44.7	1564
	R	50	8.5	7.5	19.9	17.4	5.8	1.3	1639
34015	L	90	8.5	6.0	18.4	15.6	6.0	9.6	1426
	R	18	7.8	7.4	20.8	17.8	45.9	2.3	1655
11442	L	7	15.9	15.8	29.1	27.6	28.2	26.5	1602
	R	70	7.9	6.1	25.2	20.8	15.2	2.5	1781
34090	L	23	13.7	11.1	21.8	16.8	-7.4	0.0	1524
	R	80	11.5	7.8	19.3	15.8	1.9	2.7	1396

Table E.13 Dataset for Chapter 4: Tibiofemoral kinematics, strain, and quadriceps force for 20 knees for first pivot trial

Donor ID	Leg Type	Trial #	Peak Relative Anterior Tibial Translation (mm)	Peak Relative Internal Tibial Rotation (deg)	Peak AM-ACL Relative Strain (%)	Peak Quadriceps Force (N)
32381	L	6	6.3	13.7	5.6	1234
	R	6	8.4	16.9	9.6	1819
61535	L	6	6.8	18.3	0.9	2157
	R	3	4.2	19.8	5.7	1455
33449	L	6	7.7	19.8	8.0	1397
	R	5	8.3	20.2	11.5	1683
33812	L	6	5.7	17.2	5.8	1548
	R	6	7.6	17.5	12.5	1407
72780	L	6	6.4	17.2	9.9	1863
	R	6	8.0	19.8	3.8	1408
42263	L	6	9.5	18.2	4.9	1457
	R	6	7.6	19.5	13.7	1980
33913	L	10	8.1	21.8	4.5	1603
	R	6	6.2	17.1	3.5	1412
34015	L	6	6.3	15.8	8.6	1361
	R	6	6.7	19.0	5.0	1574
11442	L	6	6.3	27.3	1.5	1575
	R	6	4.8	21.4	6.5	1355
34090	L	6	6.8	14.1	11.8	1621
	R	6	7.1	17.0	6.5	1222

Table E.14 Dataset for Chapter 4: Tibiofemoral kinematics, strain, and quadriceps force for 20 knees for last non-pivot trial

Donor ID	Leg Type	Peak Relative Anterior Tibial Translaion (mm)	Peak Relative Internal Tibial Rotation (deg)	Peak AM-ACL Relative Strain (%)	Peak Quadriceps Force (N)
32381	L	3.6	3.6	3.6	1296
	R	4.3	4.7	1.0	1753
61535	L	4.6	7.8	1.6	1922
	R	3.1	3.7	2.9	1575
33449	L	4.1	6.0	4.4	1577
	R	5.5	8.4	5.2	1829
33812	L	2.8	5.0	4.2	1774
	R	3.3	5.3	6.6	1416
72780	L	3.8	6.3	7.7	1760
	R	4.2	4.6	2.2	1414
42263	L	4.7	4.9	1.8	1353
	R	4.7	5.9	9.3	1751
33913	L	5.2	9.1	6.1	1462
	R	5.1	6.6	2.7	1275
34015	L	5.1	6.0	6.2	1294
	R	5.1	6.1	3.2	1440
11442	L	4.5	8.4	1.4	1704
	R	4.1	4.8	3.6	1472
34090	L	4.2	4.5	2.3	1541
	R	4.7	2.9	5.1	1317

Table E.15 Dataset for Chapter 5: Lateral tibial slope measurements for 11 knees using the midpoint method, circle method, and full tibia method

Donor ID	Height (cm)	Lateral Tibial Slope (deg)				
		Midpoint Method (20 cm)	Midpoint Method (15 cm)	Midpoint Method (10 cm)	Circle Method	Full Tibia Method
FA188L	165.1	9.1	5.4	4.6	1.1	3.3
FA263L	160.0	11.9	10.7	11.7	6.9	9.9
FA263R	160.0	12.5	12.5	10.8	7.8	8.2
FA266L	157.5	8.1	6.7	6.7	3.8	8.3
FA452L	162.6	11.6	9.1	10.7	8.7	10.2
FA660L	157.5	6.8	7.0	8.3	3.2	5.9
FA827L	165.1	6.7	6.7	6.7	6.0	5.7
MA381L	182.9	9.1	7.9	7.9	3.5	6.7
MA381R	182.9	9.7	5.7	7.0	5.7	7.3
MA535L	172.7	8.5	7.3	6.5	1.9	5.9
MA535R	172.7	4.3	1.4	1.4	0.0	4.0

Table E.16 Dataset for Chapter 5: Lateral tibial slope measurements for an additional 29 knees using the midpoint method and circle method

Donor ID	Height (cm)	Lateral Tibial Slope (deg)			
		Midpoint Method (20 cm)	Midpoint Method (15 cm)	Midpoint Method (10 cm)	Circle Method
F33283L	167.6	10.7	6.8	11.4	7.4
F33291L	172.7	11.5	10.2	8.8	4.3
F33313L	175.3	4.5	3.3	1.8	4.0
F33379R	154.9	12.7	12.1	8.7	6.1
F33434L	167.6	8.7	7.5	7.5	0.0
F33462L	165.1	7.8	6.7	4.9	7.9
F33524L	172.7	14.4	11.9	14.1	8.4
F33540L	172.7	10.9	8.7	7.9	7.0
F33603L	152.4	13.5	13.5	12.6	12.7
F33603R	152.4	13.2	12.4	14.7	12.3
F33681R	162.6	12.1	10.4	11.1	5.8
F33704L	167.6	7.3	5.4	8.2	4.1
F33704R	167.6	10.8	9.0	6.8	4.1
F33781L	154.9	9.4	9.5	10.7	2.3
F33784L	157.5	5.4	3.3	0.5	1.0
F33784R	157.5	4.5	4.2	3.2	0.0
F33913L	167.6	9.7	7.8	7.1	7.1
F33913R	167.6	8.6	5.8	5.2	7.7
F33971R	170.2	8.7	8.2	8.0	6.7
FA971L	157.5	8.8	8.8	11.1	8.1
FA971R	157.5	3.4	1.8	2.9	6.6
M33449L	188.0	13.3	13.3	13.3	8.2
M33449R	188.0	17.7	16.4	14.8	8.3
M33614L	180.3	9.4	7.5	5.6	5.3
M33647R	170.2	8.9	7.7	8.1	3.3
M33789L	180.3	15.5	14.2	10.2	2.1
M33789R	180.3	9.7	9.7	6.3	2.1
M33812L	177.8	16.2	10.0	11.3	5.2
M33812R	177.8	14.2	11.0	13.5	6.5

Table E.17 Dataset for Chapter 6: Morphologic characteristics and peak AM-ACL relative strain during a 2*BW simulated pivot landing for 29 knees

Donor ID	Peak AM-ACL Relative Strain (%)	Morphologic Characteristics				
		ACL Cross-Sectional Area (mm^2)	Lateral Tibial Slope (deg)	Medial Tibial Slope (deg)	Medial Tibal Depth (mm)	Notch Width Index
M33614L	0.7	48.1	3.2	3.4	3.6	0.267
F33291R	5.6	20.2	5.4	6.5	2.3	0.280
M33160R	4.5	41.5	3.6	6.5	0.7	0.287
F33540R	8.0	24.7	5.1	2.2	1.0	0.233
F33085L	1.3	27.1	2.6	6.1	1.8	0.256
F33462L	7.9	21.7	8.0	5.0	0.8	0.291
F33434	5.0	21.2	0.8	4.3	0.9	0.274
F33272L	8.8	22.4	6.7	5.2	1.2	0.266
M32901R	7.9	27.5	5.0	8.4	3.1	0.268
M33400L	3.6	37.0	1.4	4.4	3.2	0.249
M33105R	2.4	31.8	4.8	2.6	2.1	0.267
F33283R	8.1	16.7	6.1	2.3	2.3	0.267
M33606L	2.4	40.3	5.4	6.3	2.4	0.241
M33610L	3.3	26.9	5.9	4.0	2.5	0.251
M32820R	2.5	42.9	2.7	3.0	2.6	0.260
F33313R	4.8	25.8	5.7	3.6	1.8	0.270
M33538	2.5	33.2	5.4	-1.1	2.4	0.277
FA266L	10.6	20.5	6.9	7.0	2.1	0.219
FA827L	7.3	19.6	7.5	8.6	2.5	0.229
F33603L	4.8	32.0	2.8	-2.4	3.1	0.293
F33291L	1.5	29.9	5.8	5.5	3.1	0.308
F33283L	7.2	22.7	5.7	1.5	3.4	0.232
F33971R	7.9	28.0	8.1	5.8	2.3	0.273
FA660L	6.2	28.9	5.1	5.7	0.3	0.257
F33955R	3.4	27.4	2.8	6.6	3.5	0.294
F33462L	3.5	26.0	6.7	6.6	1.4	0.286
F33434L	5.2	29.9	4.4	1.7	1.1	0.280
F33681R	3.1	25.2	5.4	3.6	3.1	0.218
F33272R	10.7	21.5	8.4	4.1	2.6	0.221